Velocity/Shape Estimation Algorithm Using Tracking Filter and Data Fusion of Dual Doppler Radar Interferometers

Kenshi Saho*, Masao Masugi
Department of Electronic and Computer Engineering, Ritsumeikan University, Kusatsu, Japan.

* Corresponding author. Tel.: +77-561-3483; email: saho@fc.ritsumei.ac.jp
Manuscript submitted October 7, 2014; accepted August 2, 2015.
doi: 10.17706/ijcee.2015.7.5.283-295

Abstract: An algorithm is proposed for estimating the shape and velocity of a moving target using dual Doppler radars. The proposed algorithm estimates a target velocity and orbit with a fusion of parameters measured by the dual Doppler radar interferometers and the α-β-γ tracking filtering. The accurate shape is then estimated by motion compensation using the estimated velocities. Numerical simulations verify that the proposed algorithm achieves accurate and real-time velocity/shape estimation. The root-mean-square error for velocity estimation is 1.20 cm/s and for shape estimation is 0.317 mm, which corresponds to 1/237 of the nominal resolution determined by the radar bandwidth.

Key words: Doppler radar interferometer, velocity and shape estimation, data fusion, α-β-γ tracking filter.

1. Introduction

Remote monitoring systems for robots and Intelligent Transporting Systems have become increasingly important. For such systems, radar techniques have been developed and applied because of their robustness and high-resolution capability compared with other sensors such as cameras. The main function of conventional radar systems is the detection of presence and positioning with accuracies of the order of 10 cm to 1 m [1], [2]. However, the acquisition of more detailed motion and shape information are promising opportunities in advanced monitoring systems. For this purpose, although many high-resolution tracking and imaging algorithms have been proposed [3], [4], most advanced systems require a large number of antennas.

To resolve these problems, shape/motion estimation techniques using small numbers of radars have recently been studied and developed [5]-[7]. However, their resolution is insufficient and/or excessive computational resources and relatively large calculation times are required for these applications. To realize the coexistence of rapid/simple calculation and accuracy, we proposed a method to estimate an orbit of scatterers with a Doppler radar interferometer [8]. This method achieved real-time imaging of the orbit of a person walking using three fixed antennas and Doppler effect-based target separation and positioning. However, we cannot estimate detailed velocity and shape using only a single Doppler radar interferometer. Although we have already proposed a shape estimation algorithm with three interferometers [9], its parameter setting and data fusion of interferometers are empirically conducted. Consequently, its effectiveness and versatility are not verified and a simpler system using only two interferometers is considered as a solution.

This paper proposes an algorithm to estimate the velocity and shape of a moving target using dual Doppler radar interferometers. The proposed algorithm is composed of three processes: data fusion, tracking filtering, and shape estimation. With the data fusion of the interferometers, we estimate the accurate velocity for each time interval. Smoothing of velocities and positions over time is then conducted using an α-β-γ tracking filter [10] assuming both position and velocity measurements. The proposed algorithm designs optimal parameters in the data fusion and tracking filtering processes considering the shape estimation. Finally, the shape is estimated using motion compensation and the estimated velocities. Numerical simulations verify that the proposed method achieves accurate velocity/shape estimation with four antennas. Moreover, we show the robustness and validity of the proposed algorithm.

2. System Model and Measurement with Doppler Radar Interferometers

Fig. 1 shows a model of our system. We deal with a two-dimensional problem in the xy plane for simplicity. A single moving target with a clear boundary is observed by dual Doppler radar interferometers. Interferometer A is located at $\mathbf{x}_{\mathrm{IA}} = (X_{\mathrm{A}}, 0)$ and interferometer B at $\mathbf{x}_{\mathrm{IB}} = (X_{\mathrm{B}}, 0)$. Each interferometer is composed of two mono-static antennas whose separation is d, which is set to a small value of the order of millimeters to realize both small physical size and wide-range measurements.

Position and radial velocity are measured at each interferometer using the imaging method described in [8]. The transmitted signal is the raised-cosine pulse $W_{\mathrm{rc}}(t)$ with a bandwidth of B and a center frequency of f_0. The radar repeats the pulse transmissions with an interval of T. The received signal at the k-th pulse transmission is:

$$r_k(t) = W_{\mathrm{rc}}(t-\tau_k)e^{j2\pi(f_0 \pm f_{\mathrm{d}k})(t-\tau_k)}, \tag{1}$$

where τ_k is delay of the pulse corresponding to the range (the distance between the interferometer and a scatterer on the target) and $f_{\mathrm{d}k}$ is the Doppler shift corresponding to the radial velocity $v_{\mathrm{d}k}$. These are expressed as $\tau_k = 2R_k/c$ and $f_{\mathrm{d}k} = 2f_0 v_{\mathrm{d}k}/c$, where c is the speed of light. The Doppler radar can measure the range R_k and radial velocity $v_{\mathrm{d}k}$ of the scatterers on the target at each time instance kT from (1). Moreover, the interferometer measures the direction-of-arrival using the range difference between the two antennas δR_k, which is determined by $\varphi_k = \mathrm{Sin}^{-1}(\delta R_k/d)$. The details of the estimation methods for τ_k, $f_{\mathrm{d}k}$, and δR_k are explained in [8]. The radar using these methods is called the Doppler radar interferometer.

Interferometer A obtains $(R_{\mathrm{A}k}, v_{\mathrm{dA}k}, \varphi_{\mathrm{A}k})$ and interferometer B obtains $(R_{\mathrm{B}k}, v_{\mathrm{dB}k}, \varphi_{\mathrm{B}k})$. The position of the scatterer measured by interferometer A is obtained as $\mathbf{x}_{\mathrm{oA}k} = (x_{\mathrm{oA}k}, y_{\mathrm{oA}k}) = (R_{\mathrm{A}k}\cdot\sin\varphi_{\mathrm{A}k} + X_{\mathrm{A}}, R_{\mathrm{A}k}\cdot\sin\varphi_{\mathrm{A}k})$. Similarly, $\mathbf{x}_{\mathrm{oBA}k} = (x_{\mathrm{oB}k}, y_{\mathrm{oB}k})$ is also obtained. Thus, the dual Doppler radar interferometer measures the position and radial velocity $(\mathbf{x}_{\mathrm{oA}k}, v_{\mathrm{dA}k})$ and $(\mathbf{x}_{\mathrm{oB}k}, v_{\mathrm{dB}k})$. The objective of this study is accurate estimation of velocity and shape using these measured parameters.

3. Problems of Conventional Methods

3.1. Imaging with Single Doppler Radar Interferometer

In [8], we achieved imaging of human outlines using the superposition of the orbits of scatterers estimated using a single Doppler radar interferometer. The velocity of the scatterer can be estimated by the time-derivative operation. However, strict velocity information of the target is not obtained using only a single interferometer. This is because the Doppler radar interferometer can measure position and radial velocity not of the center of the target, but the scatterer on the target. Fig. 2 illustrates an example of the target motion and the orbit of the scatterer measured with a single interferometer. The motions of the target and scatterer are different. Therefore, the target velocity is not estimated using the orbit of the

scatterer. Moreover, we cannot distinguish between the case of Fig. 2 and a case of a point-like target moving along the same orbit as the scatterer in Fig. 2. Thus, the single interferometer cannot estimate the velocity and shape of the target.

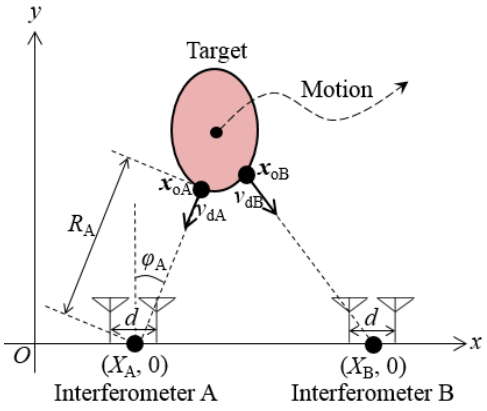

Fig. 1. System model.

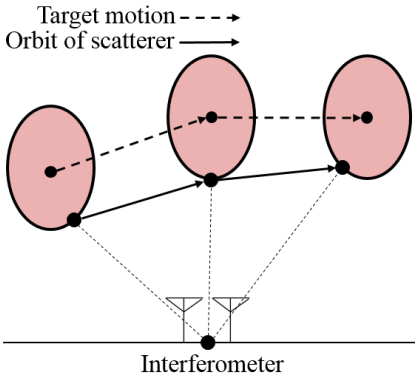

Fig. 2. Target motion and orbit of a scatterer measured with a single interferometer.

3.2. Shape Estimation with Motion Compensation

In radar imaging, the usual method for estimating target shape is to compensate for the motion of the target on the acquired scatterer position, which is expressed as [7]:

$$\mathbf{x}_{\mathrm{Sh}k} = \mathbf{x}_{\mathrm{sc}k} - \sum_{i=0}^{k} \mathbf{v}_{\mathrm{T}i} T \,, \tag{2}$$

where $\mathbf{x}_{\mathrm{sh}k}$, $\mathbf{x}_{\mathrm{sc}k}$, and $\mathbf{v}_{\mathrm{T}k}$ are the target shape, the orbit of scatterers, and the target velocity. Equation (2) indicates that accurate velocity estimation is required for accurate shape estimation. However, a single Doppler radar interferometer cannot estimate the target velocity as described in the previous section. Although various effective shape estimation algorithms (without Doppler radars) are proposed, these require many antennas and/or time-consuming calculations [6], [7]. As a solution to this problem, we proposed an imaging algorithm using three Doppler radar interferometers [9]. However, this algorithm includes ad hoc processing and empirical parameter settings. Moreover, an imaging system composed of a simpler system has promise in our assumed applications.

4. Proposed Algorithm

To resolve the above problems, an algorithm is proposed to estimate the velocity and shape of a moving target based on a tracking filter and data fusion of two Doppler radar interferometers. The outline of the proposed algorithm is:

1) Measurements of ($\mathbf{x}_{\mathrm{oA}k}$, $v_{\mathrm{dA}k}$) and ($\mathbf{x}_{\mathrm{oB}k}$, $v_{\mathrm{dB}k}$): We use the dual Doppler radar interferometers as described in Section 2.
2) Data fusion of ($\mathbf{x}_{\mathrm{oA}k}$, $v_{\mathrm{dA}k}$) and ($\mathbf{x}_{\mathrm{oB}k}$, $v_{\mathrm{dB}k}$): This process realizes accurate velocity estimation because radial velocities are used, measured by the Dual Doppler radars.
3) Tracking filtering: This process enhances the estimation accuracy of the position and velocity using the α-β-γ filters, which are optimally designed.
4) Shape estimation: Motion compensation similar to (2) is applied.

Details of each procedure and the parameter design are explained in the following subsections.

4.1. Shape Estimation with Motion Compensation

Using data fusionof the dual Doppler radar interferometers, the target velocity at each time instance kT can be estimated by the following two methods:

- The velocity vector $\mathbf{v}_{e1k}$ is obtained using a combination of two radial velocities as:

$$\mathbf{v}_{e1k} = \begin{pmatrix} v_{dAk} & v_{dBk} \end{pmatrix} \begin{pmatrix} u_{Axk} & u_{Bxk} \\ u_{Ayk} & u_{Byk} \end{pmatrix}^{-1} \tag{3}$$

where $\mathbf{u}_{Ak}= (u_{Axk}, u_{Ayk})$ is the unit vector in the radial direction calculated by $(\mathbf{x}_{IA} - \mathbf{x}_{oAk})/|\mathbf{x}_{IA} - \mathbf{x}_{oAk}|$. $\mathbf{u}_{Bk}$ is similarly calculated.

- The mean position of the scatterers estimate using the interferometers is calculated as:

$$\mathbf{x}_{ek} = \eta \mathbf{x}_{oAk} - (1-\eta)\mathbf{x}_{oBk} \tag{4}$$

where $0 < \eta < 1$is the dimensionless parameter to control the weight and is determined by estimation accuracy of the interferometers. The velocity is estimated by the time derivative of this as

$$\mathbf{v}_{e2k} = (\mathbf{x}_{ek} - \mathbf{x}_{ek-1}) / T . \tag{5}$$

The proposed algorithm estimates the velocity using $\mathbf{v}_{e1k}$ and $\mathbf{v}_{e2k}$ as

$$\mathbf{v}_{ek} = \theta \mathbf{v}_{e1k} + (1-\theta)\mathbf{v}_{e2k} \tag{6}$$

where $0 < \theta < 1$ is the dimensionless parameter to determine the weight of each estimation method. The design of parameters η and θ is described in Section 4.3.

4.2. α-β-γ Tracking Filtering and Shape Estimation

To achieve accurate shape estimation, the tracking filter is applied for the smoothing and prediction of position and velocity. The proposed algorithm uses the α-β-γ filter, which is known as a simple and effective tracking filter assuming a constant acceleration during the sampling interval [10]. By using the position and velocity estimated in the data fusion process, α-β-γ filter tracking is conducted by the following equations:

$$\mathbf{x}_{pk} = \mathbf{x}_{sk-1} + T\mathbf{v}_{sk-1} + (T^2/2)\mathbf{a}_{sk-1}, \tag{7}$$

$$\mathbf{v}_{pk} = \mathbf{v}_{sk-1} + T\mathbf{a}_{sk-1}, \tag{8}$$

$$\mathbf{a}_{pk} = \mathbf{a}_{sk-1}, \tag{9}$$

$$\mathbf{x}_{sk} = \mathbf{x}_{pk} + \alpha\left(\mathbf{x}_{ek} - \mathbf{x}_{pk}\right), \tag{10}$$

$$\mathbf{v}_{sk} = \mathbf{v}_{pk} + \beta\left(\mathbf{v}_{ek} - \mathbf{v}_{pk}\right) \tag{11}$$

$$\mathbf{a}_{sk} = \mathbf{a}_{pk} + (\gamma / \mathrm{T})\left(\mathbf{v}_{ek} - \mathbf{v}_{pk}\right) \tag{12}$$

where $\mathbf{x}_{pk} = (x_{pk}, y_{pk})$ is the predicted position, $\mathbf{x}_{sk} = (x_{sk}, y_{sk})$ is the smoothed (estimated) position, $\mathbf{v}_{pk} = (v_{pxk}, v_{pyk})$ is the predicted velocity, $\mathbf{v}_{sk} = (v_{sxk}, v_{syk})$ is the smoothed (estimated) velocity, $\mathbf{a}_{pk} = (a_{pxk}, a_{pyk})$ is the predictedacceleration, and α, β, and γ are filter gains. The filter gains are often set between 0 and 1. Note that this filter uses the measured velocity, which is different from the general α-β-γ filter assuming only position measurement. From the above filtering process, the estimated velocity $\mathbf{v}_{sk}$ is obtained. In addition, we also estimate the smoothed position of each interferometer $\mathbf{x}_{sAk}$ and $\mathbf{x}_{sBk}$ by replacing $\mathbf{x}_{ek}$ to $\mathbf{x}_{oAk}$ and $\mathbf{x}_{oBk}$ in (10).

Similar to (2), the target shape estimated from the interferometer A is expressed as:

$$\mathbf{x}_{ShAk} = \mathbf{x}_{sAk} - \sum_{i=0}^{k} \mathbf{v}_{si} T \tag{13}$$

Similarly, $\mathbf{x}_{ShBk}$ is also estimated and the target shape is estimated using the superposition of $\mathbf{x}_{ShAk}$ and $\mathbf{x}_{ShBk}$.

In the tracking filtering process, the design parameters are the filter gainsα, β, and γ. The proposed algorithm uses optimum gains determined by error analysis of the α-β-γ filter. Analysis results and reasonable parameter design methods are described in the following subsections.

4.3. Optimal Parameter Design Based on Error Analysis

This section analyzes the tracking errors and describes optimal parameter design. As shown in (13), the accuracy of the velocity estimation is very important for the shape estimation. Consequently, the parameters of the proposed algorithm are set by minimizing the error of the velocity estimation in the data fusion and tracking processes. Here, for simplicity, we consider only errors in the x-axis because the results in both axes are the same. In the analysis, we assume a target moving with constant acceleration because the smoothing performance of the tracking filter is generally evaluated from the steady-state error for this type of target [11]. Using (8), (9), (11), and (12), the steady-state variance of errors of v_{xsk} is calculated as:

$$\sigma_v^2 = \mathrm{E}[(v_{sxk} - v_{txk})^2] = \frac{2\beta^2 + 2\gamma - 3\beta\gamma}{\beta(4 - 2\beta - \gamma)} B_v \tag{14}$$

where v_{txk} is the true velocity, E[ ] indicates the mean, and B_v is the variance of the error of v_{ek} calculated using (4)–(6) as:

$$B_v = \mathrm{E}[(v_{ek} - v_{tk})^2] = \theta^2 B_{ve1} + \frac{2(1-\theta)^2}{T^2}[\eta^2 B_{xA} + (1-\eta)^2 B_{xB}], \tag{15}$$

where B_{ve1}, B_{xA}, and B_{xB} are the error variances of v_{e1k}, x_{oAk}, and x_{oBk}. The derivation of (14) is given in Appendix A.

First, we investigate the optimal β. Equation (14) shows that σ_v^2 is convex downward for $0 < \beta < 1$. Thus, with $\partial\sigma_v^2/\partial\beta = 0$,we have the optimal relationship of β andγ as:

$$\beta = \frac{\gamma + (\gamma - 2)\sqrt{\gamma}}{2(\gamma - 1)} \tag{16}$$

Next, we minimize B_v to similarly design η and θ. With $\partial B_v/\partial\eta=0$, η is calculated as:

$$\eta = \frac{1}{1+(B_{xA}/B_{xB})} \tag{17}$$

With $\partial B_v/\partial\theta=0$ and (17) being satisfied, we also have:

$$\theta = \frac{2}{2+(T^2 B_{ve1}/B_x)} \tag{18}$$

where,

$$B_x = \frac{1}{1/B_{xA}+1/B_{xB}} \tag{19}$$

Thus, η and θ are easily designed based on the performance of the interferometers.

Moreover, the optimal α is designed using the steady-state errors of the smoothed position. With the same procedure as for σ_v^2, the error variance of x_{Ask} is derived as:

$$\sigma_x^2 = \frac{\alpha}{2-\alpha}B_{xA} + \frac{(1-\alpha)^2 f(\alpha,\beta,\gamma)}{2\alpha\beta(2-\alpha)(4-2\beta-\gamma)(\alpha^2+\alpha\beta+\gamma-\alpha\gamma-\alpha^2\beta)}T^2 B_v \tag{20}$$

where,

$$f(\alpha,\beta,\gamma) = \alpha^2(4\beta-2\beta\gamma-\gamma^2+4\gamma)+\alpha(6\beta^2\gamma-4\beta^3+8\beta^2+3\beta\gamma^2-16\beta\gamma-2\gamma^2+8\gamma)-4\beta\gamma^2+2\beta\gamma(4-\gamma). \tag{21}$$

We determine the optimal α by minimizing σ_x^2 under the condition that β and γ are constant. Because of its complexity, the derivation and minimization processes of σ_x^2 are omitted. The procedure is same as for σ_v^2.

The proposed algorithm designs the optimal α, β, η, and θ using (16)–(21) from γ and the ratio of noise variances of the measurement parameters. In practice, the noise variances are easily determined based on the performance of the radars. We discuss the appropriate setting of γ in the next subsection.

4.4. Discussion for Parameter γ

This subsection clarifies the role of γ and discusses its design criterion. In the previous subsection, we assumed a target moving with constant acceleration to analyze smoothing performance. However, even in noiseless cases, the α-β-γ filter cannot estimate position and velocity for a target moving with a jerk without errors. For instance, in the tracking of a target moving with a constant jerk, bias error occurs. When $v_{ok}=JT^2/2$ (J is the jerk), the steady-state bias error for the smoothed velocity is calculated using (8), (9), (11), and (12) as:

$$e_{sv} = \lim_{k\to\infty}(v_{ok}-v_{sk}) = \frac{1-\beta}{\gamma}JT^2 \tag{22}$$

The derivation of (22) is given in Appendix B. In addition, the steady-state bias error for the predicted

velocity is also derived using a similar procedure to (22) as:

$$e_{pv} = \lim_{k\to\infty}(v_{ok} - v_{pk}) = JT^2 / \gamma \tag{23}$$

Equations (22) and (23) mean thatγ is dominant for these bias errors and that large γ reduces these errors. However, as indicated in (14), large γ degrades the smoothing performance. This means there is a trade-off between these errors and σ_v^2. Based on this consideration, we should set appropriate γ based on the predicted and/or measured target motion. For example, when the target jerk is estimated as being small, we should set a relatively small γ to conduct sufficient smoothing. Otherwise, we should set a relatively large γ to track a target having a complicated motion including a relatively large jerk.

4.5. Summary and Procedure of Proposed Algorithm

The procedure for the proposed algorithm is summarized in Fig. 3. In the proposed algorithm, we set γ, $B_{ve1}/B_{x,}$ and B_{xA}/B_{xB} based on the performance of the radars and motion of the assumed target. The optimal parameters in the data fusion and tracking processes are then set automatically using the derived equations. The target shape is estimated using the orbit of scatterers and the velocity that are optimally estimated using data fusion and the α-β-γ tracking filtering.

5. Performance Evaluation with Numerical Simulations

5.1. Shape Estimation Example

In this section, we validate the performance of the proposed imaging algorithm using numerical simulations. The shape and motion of the target and the locations of interferometers are shown in Fig. 4. The target is an ellipse with a major axis of 4 cm and minor axis of 3 cm. The locations of interferometers are $\mathbf{x}_{IA}$ = (0, 0) and $\mathbf{x}_{IB}$ = (0.5 m, 0). The separation of the antennas is d = 1.07 mm, this corresponds to a half-wavelength of the transmitting signal. The parameters of the transmitting signal are the bandwidth B = 2 GHz and the center frequency f_0 = 140 GHz, and these are nominal values for the next generation of near field radar systems. The sampling interval of the measured signal T = 10 ms. The true motion of the target center is (x_{tk}, y_{tk}) = $(0.5 - 0.045kT + 5\times10^{-5}\cdot(kT)^3,\ 0.9 - 0.003(kT)^2)$. The received signals are calculated using ray-tracing and adding white Gaussian noise. In this section, we set a maximum signal to noise ratio (SNR) of the received signals in the time domain of 30 dB. Based on the sensing performance, we set η = 0.5 and θ = 0.914 using (22)–(24).

Fig. 5 shows the result of the velocity estimation in the x-axis using the proposed algorithm with γ = 0.1, and the conventional methods using a single interferometer and only (3) (the velocity is estimated as the time-derivative of the position of the scatterer). As shown in this figure, the proposed algorithm realizes reasonable velocity estimation. The root-mean-square (RMS) error of the velocity with the proposed algorithm is 1.20 cm/s. This is better than the other method; the RMS velocity errors with a single interferometer and only (3) are 3.90 and 2.08 cm/s, respectively. Fig. 6 shows the shape estimation results for each method. As shown in this figure, the proposed algorithm achieves accurate shapeestimation compared with other methods. In contrast, the method using only a single interferometer fails to estimate the target shape. This is because the estimated velocity is not the target velocity as described in Section 3. Moreover, by comparison with Fig. 6(b) and Fig. 6(c), the proposed algorithm realizes reliable estimation by the optimal smoothing using the α-β-γ filter. The RMS errors of the shape in Fig. 6(b) and Fig. 6(c) are 0.690 and 0.317 mm. Note that 0.317 mm corresponds to 1/237 of the nominal resolution determined by B of 2 GHz (=75 mm).

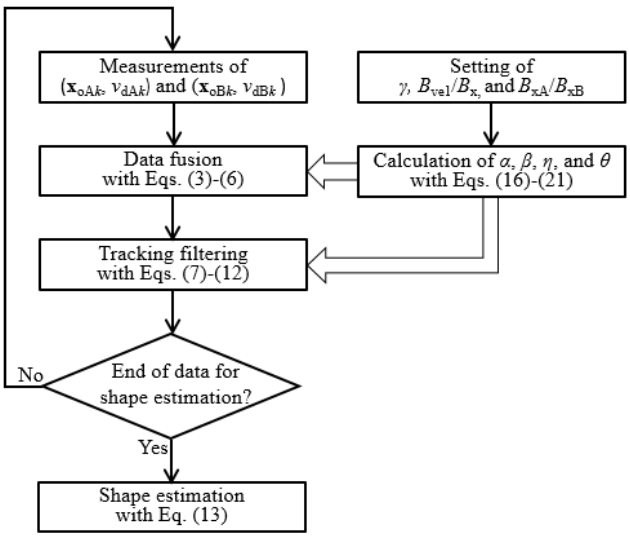

Fig. 3. Procedure of the proposed algorithm.

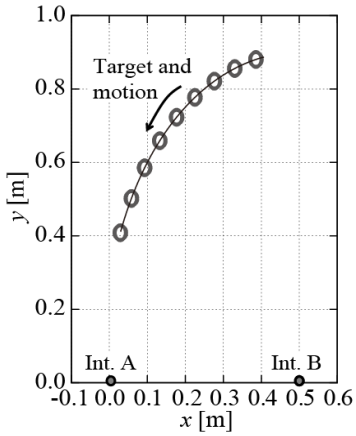

Fig. 4. Situation of simulation in Section 5.

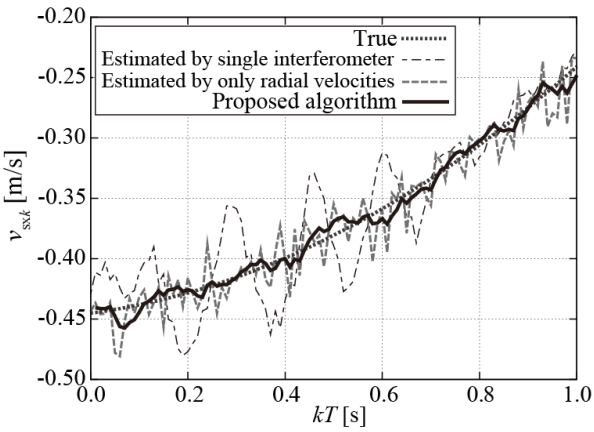

Fig. 5. Velocity estimation results in x-axis.

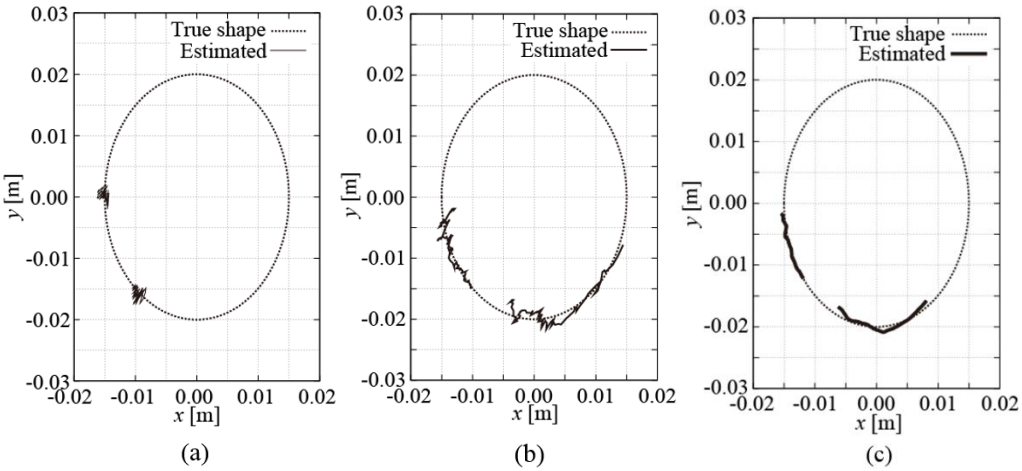

Fig. 6. Shape estimation results. (a): Single interferometer; (b): Estimated by only radial velocities; (c): Proposed algorithm.

5.2. Discussion for Design Parameters

This subsection clarifies the effectiveness of the parameter design in the proposed algorithm. This section

assumes the same situation as in the previous section (Fig. 4). Fig. 7 shows the relationship between β and the RMS velocity estimation error for γ = 0.1 using the same data as in Fig. 5, and indicates that (16) determines the optimum β. Fig. 8 shows the relationship between α and the RMS shape estimation error, and indicates that an optimum α for the shape estimation is designed using (20). In addition, we confirmed that parameters η and θ have the same tendency. These results verify that the proposed algorithm automatically determines optimal parameters.

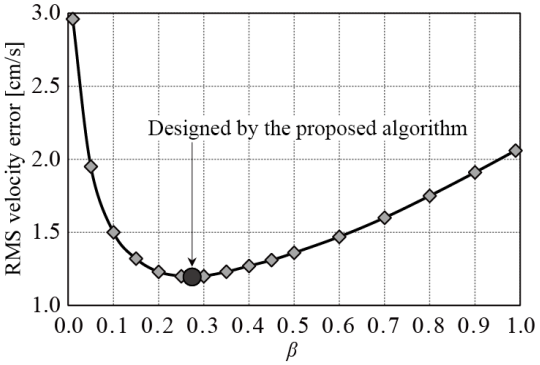

Fig. 7. Relationship between β and RMS velocity error.

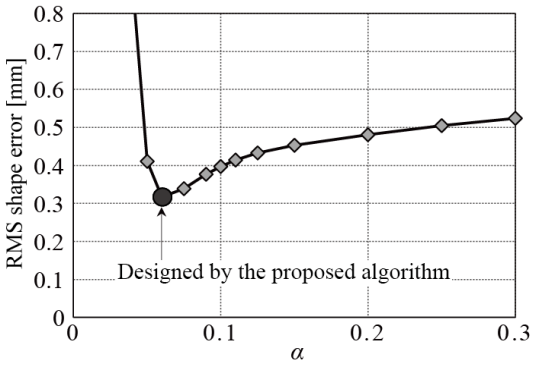

Fig. 8. Relationship between α and RMS shape error.

Considering the setting of γ, Fig. 9 shows the relationship between the RMS shape error and the parameter for the same target motion as in Fig. 4. As shown in this figure, a suitable gamma is 0.1 because the jerk of the target is relatively small. By contrast, Fig. 10 assumes a target motion of (x_{tk}, y_{tk}) = $(0.7-0.03kT+10^{-4}\cdot(kT)^3, 0.9-10^{-4}\cdot(kT)^3)$, which has a large jerk compared with the previous example.

Fig. 10 indicates that the appropriate setting range is $0.4 < \gamma < 0.6$. These results mean that the setting of γ should be conducted assuming the target jerk. However, Fig. 9 and Fig. 10 also show that the deterioration in the performance of the proposed algorithm is not as large when γ is set around the optimal values. Thus, we can easily design an appropriate γ from the assumed target motion.

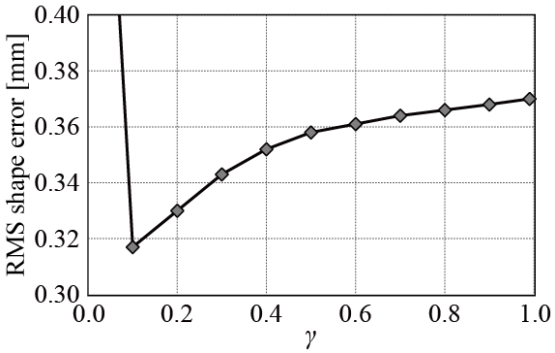

Fig. 9. Relationship between γ and RMS shape error assuming a target with a relatively small jerk.

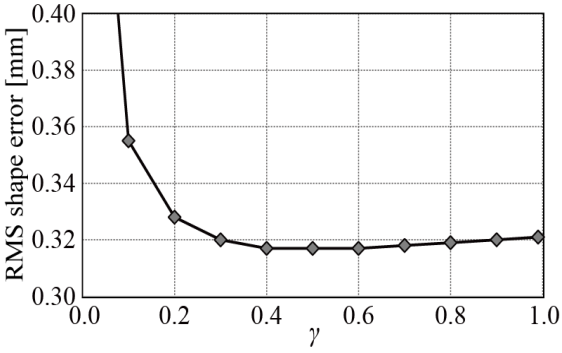

Fig. 10. Relationship between γ and RMS shape error assuming a target with a relatively large jerk.

5.3. Performance in Other Shapes and SNR Cases

This subsection shows the performance in other target shapes and SNR cases. Fig. 11 shows the relationship between the maximum SNR and the RMS shape error, and the assumed target shape. To generate Fig. 11(a), we conduct 100 Monte-Carlo simulations for each SNR. In these simulations, radar settings including parameters of the proposed algorithm and target motion are the same as in Sub-section *A*.

The target shape is an ellipse with axes L_x and L_y and slant angle ψ as shown in Fig. 11(b), and these parameters are set randomly for each simulation. The ranges of these parameters are $0 < L_x, L_y < 5$ cm and $0 \le \psi < \pi$ and a uniform distribution is assumed.

Fig. 11(a) verifies that the proposed algorithm works well for SNR ≥ 20 dB. In addition, the standard deviations of the errors in the Monte-Carlo simulations are small, at less than 0.1 mm. In contrast, large errors are confirmed for approximate SNR < 18 dB. This is because the miss-detections of the signals resulting from excessive noise lead to impulsive errors in the measurements using the interferometers. However, a SNR ≥ 20 dB is easily realized in practice by means of spectral-spread techniques [2], [8]. Consequently, the proposed algorithm is applicable even in actual situations.

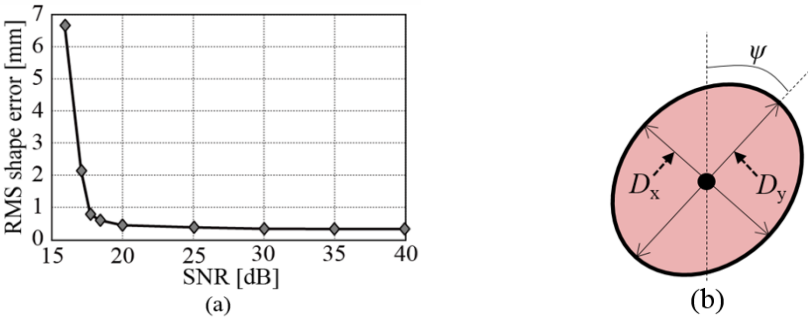

Fig. 11. Simulation for various SNRs and target shapes. (a): RMS shape error for various SNRs, (b): Assumed target shape.

6. Conclusions

This study proposes a shape and velocity estimation algorithm using dual Doppler radar interferometers. The proposed algorithm estimates an accurate target velocity using data fusion of the interferometers and an α-β-γ tracking filter. The optimum parameters were designed based on the analyses of the errors in the fusion and tracking processes. The target shape is then estimated with motion compensation using the estimated velocity. The numerical simulations verified that the proposed algorithm achieved an accurate shape and velocity estimation of the moving target in noisy environments. When the maximum SNR of the received signals is 30 dB, the RMS errors of the velocity and shape were 1.20 cm/s and 0.317 mm, which corresponds to 1/237 of the nominal range resolution of 75 mm determined by the bandwidth of 2 GHz. Moreover, we showed that the proposed algorithm works well for SNR ≥ 20 dB. However, this study assumed a single target only. Applications to multiple moving targets are important future studies.

Appendix A: Derivation of (14)

The true velocity of a constant acceleration target is expressed as $v_{tk}=v_{tk-1}+Ta_{tk}$. Thus, the velocity estimation error at time kT is expressed using (8) and (11) as:

$$v_{sxk} - v_{txk} = (1-\beta)\left[(v_{sxk-1} - v_{stk-1}) + T(a_{sxk-1} - a_{stk-1})\right] + \beta\left(v_{exk} - v_{txk}\right). \tag{24}$$

Because we can assume the errors in smoothing and measurement are uncorrelated, the variance of this error is calculated as:

$$\begin{aligned}\sigma_v^2 = \mathrm{E}[(v_{sxk} - v_{txk})^2] = (1-\beta)^2\{\mathrm{E}[(v_{sxk-1} - v_{stk-1})^2] + T\,\mathrm{E}[(a_{sxk-1} - a_{stk-1})^2] \\ + \mathrm{E}[(v_{sxk-1} - v_{stk-1})(a_{sxk-1} - a_{stk-1})]\} + \beta^2\,\mathrm{E}[(v_{exk} - v_{stk})^2].\end{aligned} \tag{25}$$

The followings are satisfied by assuming a steady-state:

$$\sigma_{\mathrm{v}}^2 = \mathrm{E}[(v_{\mathrm{sx}k} - v_{\mathrm{tx}k})^2] = \mathrm{E}[(v_{\mathrm{sx}k-1} - v_{\mathrm{st}k-1})^2], \tag{26}$$

$$\sigma_{\mathrm{a}}^2 = \mathrm{E}[(a_{\mathrm{sx}k} - a_{\mathrm{tx}k})^2] = \mathrm{E}[(a_{\mathrm{sx}k-1} - a_{\mathrm{tx}k-1})^2], \tag{27}$$

$$\sigma_{\mathrm{va}}^2 = \mathrm{E}[(v_{\mathrm{sx}k} - v_{\mathrm{tx}k})(a_{\mathrm{sx}k} - a_{\mathrm{tx}k})] = \mathrm{E}[(v_{\mathrm{sx}k-1} - v_{\mathrm{st}k-1})(a_{\mathrm{sx}k-1} - a_{\mathrm{tx}k-1})], \tag{28}$$

$$B_{\mathrm{v}} = \mathrm{E}[(v_{\mathrm{ex}k} - v_{\mathrm{tx}k})^2]. \tag{29}$$

Substituting(26)-(29) into (25), we have:

$$\beta(2-\beta)\sigma_{\mathrm{v}}^2 - (1-\beta)^2(T^2\sigma_{\mathrm{a}}^2 + 2T\sigma_{\mathrm{va}}^2) = \beta^2 B_{\mathrm{v}}. \tag{30}$$

Similar to(25), we have the following by calculating E[($a_{\mathrm{sx}k}$–$a_{\mathrm{tx}k}$)²] and E[($v_{\mathrm{sx}k}$–$v_{\mathrm{tx}k}$)($a_{\mathrm{sx}k}$–$a_{\mathrm{tx}k}$)] using (8), (9), (11), and (12):

$$-(\gamma/T)^2\sigma_{\mathrm{v}}^2 + \gamma(2-\gamma)\sigma_{\mathrm{a}}^2 - (2\gamma(1-\gamma)/T)\sigma_{\mathrm{va}}^2 = (\gamma/T)^2 B_{\mathrm{v}}, \tag{31}$$

$$\gamma(1-\beta)\sigma_{\mathrm{v}}^2 - (1-\beta)(1-\gamma)T\sigma_{\mathrm{a}}^2 + (\beta+2\gamma-2\beta\gamma)\sigma_{\mathrm{va}}^2 = (\beta\gamma/T)B_{\mathrm{v}}. \tag{32}$$

By solving a linear system involving (30)–(32) for σ_{v}^2, we arrive at (14).

Appendix B: Derivation of (22)

Applying a z-transform to(8), (9), (11), and (12) and assuming a noiseless case, we obtain:

$$V_{\mathrm{p}}(z) = V_{\mathrm{s}}(z)/\mathrm{z} + TA_{\mathrm{s}}(z)/\mathrm{z}, \tag{33}$$

$$A_{\mathrm{p}}(z) = A_{\mathrm{s}}(z)/\mathrm{z}, \tag{34}$$

$$V_{\mathrm{s}}(z) = (1-\beta)V_{\mathrm{p}}(z) + \beta V_{\mathrm{t}}(z), \tag{35}$$

$$A_{\mathrm{s}}(z) = A_{\mathrm{p}}(z) + (\gamma/T)\{V_{\mathrm{t}}(z) - V_{\mathrm{p}}(z)\}. \tag{36}$$

Simplifying (33)–(36), we have:

$$V_{\mathrm{s}}(z) = \frac{z(\beta z + \gamma - \beta)}{z^2 + (\beta+\gamma-2)\mathrm{z} - \beta + 1} V_{\mathrm{t}}(z). \tag{37}$$

Here, we assume the target is moving with constant jerk$J$, and the true velocity and its z-transform is:

$$V_t(z) = \mathrm{Z}\left[J(kT)^2 / 2 \right] = \frac{z(z+1)}{2(z-1)^3} JT^2, \tag{38}$$

where Z[ ] indicates the z-transform. Using (37) and (38), the z-transform of the error $v_{tk}-v_{sk}$ is calculated as:

$$E_s(z) = V_t(z) - V_s(z) = \frac{(1-\beta)(z-1)^2}{z^2 + (\beta+\gamma-2)z - \beta + 1} \cdot \frac{z(z+1)}{2(z-1)^3} JT^2 = \frac{z(1-\beta)(z+1)}{2(z-1)\{z^2 + (\beta+\gamma-2)z - \beta + 1\}} JT^2. \tag{39}$$

Using the final value theorem, we arrive at:

$$e_{sv} = \lim_{z \to 1} (z-1) E_s(z) = \frac{1-\beta}{\gamma} JT^2. \tag{40}$$

Acknowledgment

This work was supported in part by the Ministry of Internal Affairs and Communications of Japan and the Japan Society for the Promotion of Science KAKENHI Grant No. 26880023.

References

[1] Wang, Y., Liu, Q., & Fathy, A. E. (2013). Cw and pulse-doppler radar processing based on fpga for human sensing applications. *IEEE Trans. Geosci. Remote Sens.*, *51,* 3097-3107.

[2] Stephan, A., Baudais, J. Y., & Helard, J. F. (2008). Range improvement of uwb systems using adaptive multicarrier spread-spectrum and mimo techniques. *Euro. Trans. Telecomms.*, *19,* 589-599.

[3] Jovanoska, S., & Thoma, R. (2012). Multiple target tracking by a distributed UWB sensor network based on the PHD filter. *Proceedings of Conf. Information Fusion* (pp. 1095-1102).

[4] Zhuge, X., & Yarovoy, A. G. (2011). A sparse aperture MIMO-SAR-based UWB imaging system for concealed weapon detection. *IEEE Trans. Geosci. Remote Sens.*, *49,* 509-517.

[5] Fogle, O. R., & Rigling, B. D. (2012). Micro-range/micro-doppler decomposition of human radar signatures. *IEEE Trans. Aero. Elec. Sys.*, *48,* 3058-3072.

[6] Onojima, S., Arima, Y., & Hirose, A. (2014). Millimeter-wave security imaging using complex-valuedself-organizing map for visualization of moving targets. *Neurocomputing, 134,* 247-253.

[7] Sakamoto, T., Matsuki, Y., & Sato, T. (2012). Method for the three-dimensional imaging of a moving target using an Ultra-Wideband radar with a small number of antennas. *IEICE Trans. Commun.*, *E95-B*, 972-929.

[8] Saho, K., Sakamoto, T., Sato, T., Inoue, K., & Fukuda, T. (2013). Pedestrian imaging using UWB doppler radar interferometry. *IEICE Trans. Commun.*, *E96-B*, 613-623.

[9] Yamazaki, H., Saho, K., & Sato, T. (2013). Accurate shape estimation method for multiple moving targets with UWB Doppler radar interferometers. *Proceedings of 10th Int. Conf. Space, Aeronautical and Navig. Electron* (pp. 7-12).

[10] Tenne, D., & Singh, T. (2002). Characterizing performance of α-β-γ filters. *IEEE Trans. Aero. Elec. Sys.*, *38,* 1072-1087.

[11] Ekstrand, B. (2012). Some aspects on filter design for target tracking. *J. Control Sci. Eng.*, *Article ID 870890*.

Kenshi Saho was born in Oita, Japan in 1986. He received his B.E., M.I., and Ph.D. degrees from Kyoto University, Japan in 2008, 2010, and 2013, respectively.

Since 2014, he has been an assistant professor of the College of Science and Engineering, Ritsumeikan University. His current research interest is in signal processing for radar imaging and tracking.

Dr. Saho is a member of the IEEE, IEICE, and IEEJ. He received the best paper award from the International Symposium on Antennas and Propagation 2012 (ISAP2012) in 2012.

Masao Masugi received his B.E., M.E., and Ph.D. degrees from Keio University, Japan in 1987, 1989, and 1994, respectively.

Since 2010, he has been a professor in the College of Science and Engineering, Ritsumeikan University. His current research interests are in signal analysis in the EMC field and bio-engineering.

Dr. Masugi is a member of the IEICE and IEEJ. He received the paper presentation award from IEEJ in 1992.